Retrieval of chlorophyll fluorescence from a large distance using oxygen absorption bands

Christiaan van der Tol [a,*], Tommaso Julitta [b], Peiqi Yang [a,c,h,i], Neus Sabater [d], Ilja Reiter [e], Marin Tudoroiu [f], Dirk Schuettemeyer [g], Matthias Drusch [g]

[a] *Faculty of Geo-Information Science and Earth Observation (ITC), University of Twente, 7500 AE Enschede, The Netherlands*
[b] *JB Hyperspectral Devices GmbH, Düsseldorf, Germany*
[c] *School of Geography, Nanjing Normal University, Nanjing, China*
[d] *Finnish Meteorological Institute, Erik Palménin aukio 1, 00560 Helsinki, Finland*
[e] *Centre National de la Recherche Scientifique, France*
[f] *ESA-ESRIN, via Galileo Galilei 2, 00044 Frascati (RM), Italy*
[g] *European Space Agency/ ESTEC, Noordwijk, The Netherlands*
[h] *Key Laboratory of Virtual Geographic Environment, Ministry of Education, Nanjing Normal University, Nanjing, China*
[i] *Jiangsu Center for Collaborative Innovation in Geographical Information Resource Development and Application, Nanjing, China*

ARTICLE INFO

ABSTRACT

The detection of solar induced chlorophyll fluorescence (SIF) in the field with spectrometers is based on the depth of the solar Fraunhofer or oxygen absorption lines in the upwelling radiance compared to that in the downwelling irradiance. This relative depth enables the differentiation of SIF from the reflected radiation. Recent studies have shown that if oxygen bands are used to retrieve SIF from tower-based measurements, then atmospheric correction is required. This study presents a band shape fitting (BSF) approach to retrieve both the relative optical path length (deepening) and SIF (infilling) from field measurements at the same time, using information in the measured spectral shape of the O_2 feature. This approach is an alternative to using radiative transfer process models for estimating atmospheric transmittance. The method was applied to measurements taken from 100 m elevation above a forest, yielding plausible results for SIF in the O_2A and O_2B bands. The sensitivity to combined atmospheric and instrument characteristics prohibits application at much greater distances from the surface.

1. Introduction

The emission of Solar Induced Fluorescence (SIF) by the pigment chlorophyll in terrestrial plants has been used as a probe for photosynthetic activity at local to global scale (Mohammed et al., 2019). Over the last ten years, the availability of remote sensing based SIF data has increased along with the number of hyperspectral instruments in orbit suitable for the retrieval of SIF: TANSO (GOSAT), SCIAMACHY (ENVISAT), GOME-2 (MetOp), CarbonSpec (TanSat), TROPOMI (Sentinel 5-P), and OCO-2. Three other missions, the dedicated Fluorescence Explorer (FLEX) mission and the geostationairy missions Sentinel-4 and TEMPO, are expected to provide SIF data in the coming years.

With the growing interest in the use of the signal of SIF in vegetation remote sensing the number of flux tower sites equipped with spec-

trometers for the monitoring of SIF in the field has increased too (Marrs et al., 2021). The detection of SIF is based on its contribution to the infilling of narrow absorption lines in the solar spectrum, which enables the differentiation of SIF from the much stronger reflected solar radiation. Both solar and telluric absorption lines can be used, and all current satellite retrievals (Köhler et al., 2018; Sun et al., 2018) and some of the field spectroscopy retrievals (Grossmann et al., 2018) use Fraunhofer lines caused by the solar atmosphere (SFL). Because the relative depth of the SFL is influenced by few other telluric processes besides the emission of SIF, the infilling of these lines as observed above the atmosphere can be attributed to fluorescence (Frankenberg et al., 2011). Although the O_2 absorption features produced by the atmosphere of the Earth are wider and deeper than the SFL, and they provide a stronger signal, the retrieval of SIF in the O_2 absorption bands is more complicated than in
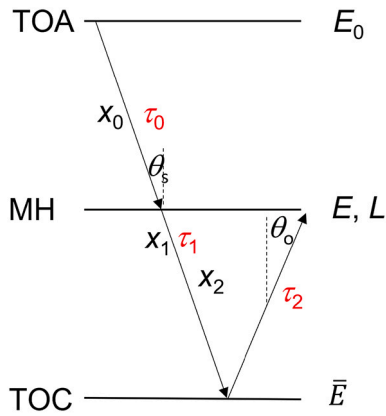

Fig. 1. Definition sketch of optical paths. Three levels are defined, Top of Atmosphere (TOA), measurement height (MH) and top of canopy (TOC). Distances between these levels are denoted by x_0, x_1 and x_2, with corresponding transmittances τ_i.

the SFL. The depth of these bands is primarily determined by the photon path length through the atmosphere of the Earth. Numerous factors affect this path length, such as aerosol concentrations, clouds, the pressure and potential temperature profile, the terrain and the surface reflectance, as discussed in detail by Guanter et al. (2010) and recently by Sabater et al. (2021). Fluorescence contributes little to the depth of the O_2 bands at TOA, and separation of its effect from that of other factors is necessary. In field installations for the retrieval of SIF, the measurements of solar irradiance E and upwelling radiance L are usually taken close to the vegetated surface, and the difference in optical path length through the atmosphere between E and L is in the order of metres. A short optical path length between E and L results in negligible additional deepening of the O_2 lines, which greatly simplifies the retrieval problem because the infilling can directly be attributed to fluorescence. The exact atmospheric path from the Sun to the sensor is then irrelevant: Only the relative depth of the absorption features in L compared to that in E matters. For this reason, some field spectroscopy measurement setups are designed for retrieval in the O_2A and O_2B bands (Aasen et al., 2019). Successful retrievals of SIF in O_2 bands have been reported with various retrieval techniques, such as the improved Fraunhofer Line Discrimination method (iFLD) and spectral fitting methods (SFM) (Cogliati et al., 2015; Cogliati et al., 2019); see also Damm et al. (2011) and Cendrero-Mateo et al. (2019) for reviews.

However, Sabater et al. (2018) showed that as little as several metres of atmosphere at sea level pressure between the fluorescent target and the sensor suffices to cause a non-negligible additional deepening of the O_2A band, and retrievals from a distance of 20 m from the target are severely affected by the additional deepening over the path from the sensor height to the surface and back to the sensor height. Measurements from croplands are typically carried out at a few meters from the surface, but retrievals from forests take usually place at more than 10 m distance from the vegetation and in such case, accounting for atmospheric effects in the retrieval of fluorescence in O_2 bands is mandatory, but no standard technique exist for this purpose.

The upwelling radiance L measured from a tower has travelled a longer distance through the atmosphere than the downwelling solar irradiance E, which causes deeper O_2 features in L than in E, thus (partly) offsetting the infilling by fluorescence in L. One can use models to correct for this additional deepening the O_2 band along the path from the measurement height to the surface and back to the measurement height (Liu et al., 2019; Sabater et al., 2018), but these models require the atmospheric profile and other atmospheric data as input. Because SIF is such a weak signal, the correction needs to be highly accurate to limit the propagation of uncertainties in the atmospheric transmittance.

Because atmosphere properties may not be known well enough to

estimate the transmittance with sufficient accuracy, we propose and investigate the Band Shape Fitting (BSF) method as an alternative approach, in which we exploit the fact that the spectral effects of additional deepening and the infilling by fluorescence on the O_2A absorption feature are different, which enables the simultaneous retrieval of the optical depth and SIF from the measured spectral with limited ancillary data inputs.

In this paper we present the algorithm, evaluate the applicability of this approach for field measurements using experimental data acquired from a tall tower above a forest, and discuss its limitations. We show that for monochromatic radiation, infilling and deepening are well separable, but effects of the instrument (the spectral response function) on the shape of the measured spectra of L and E are strong, they interfere with the fluorescence retrieval, and need to be corrected for.

2. Theory

In the following derivation, we define three heights: Top-of-Atmosphere (TOA), the measurement height (MH), and Top-of-Canopy (TOC). The source of the irradiance and fluorescence is at TOA and TOC, respectively, and all signals are measured at MH (Fig. 1). At the MH we define the upwelling radiance (L) and the downwelling irradiance (E). The fluorescence is defined at the surface, where it is emitted (F). Three optical path lengths are differentiated: x_0 is the path of the irradiance from TOA to MH, x_1 the continued path from MH to TOC, and x_2 the path of the upwelling radiance from TOC to MH. We make the strong assumptions that the extinction coefficients have identical spectral shape over the different paths x_0, x_1 and x_2, and for the time being, we do not consider that both E and L are convolutions of the true (ir) radiance with the SRF (Spectral Response Function). In other words, we treat the radiance as monochromatic. This enables the derivation of a simple relation between E and L that allows for the retrieval of F. However, we will also show that this simplification renders substantial errors in F and that correction for the instrument response function is needed.

For monochromatic radiation, the corresponding transmittances T_0, T_1 and T_2 are mathematically described as:

$$T_i = \exp(-kx_i) \tag{1}$$

where k is a wavelength dependent extinction coefficient ($k = k(\lambda)$). The irradiance measured at MH can thus be described as:

$$E = E_a T(x_0) = E_a \exp(-kx_0) \tag{2}$$

where E_a is the extraterrestrial solar radiation. The surface irradiance consists of both direct and indirect solar radiation (the latter is a diffuse flux), each with a different path length through the atmosphere from the Sun to the sensor. The effective path x_0 weights the contributions of these two components of irradiance.

The upwelling radiance L_r travels over a longer path to the MH. In absence of fluorescence ($F = 0$) it can be expressed as:

$$\pi L_r = E_a r \exp(-k(x_0 + x_1 + x_2)) \tag{3}$$

By combining Eqs. (2) and (3) we can define a relative optical path length a as follows:

$$\frac{\log \frac{\pi L_r}{r E_a}}{\log \frac{E}{E_a}} = \frac{x_0 + x_1 + x_2}{x_0} = a \tag{4}$$

The right hand side in Eq. (4) is wavelength independent, and the coefficient a is a ratio of optical path lengths of the upwelling and downwelling measurement. Thus, a linear relationship can be expected between the logarithms of L and E, and deviation from this linearity may be attributed to confounding factors including (but unfortunately not limited to) SIF.

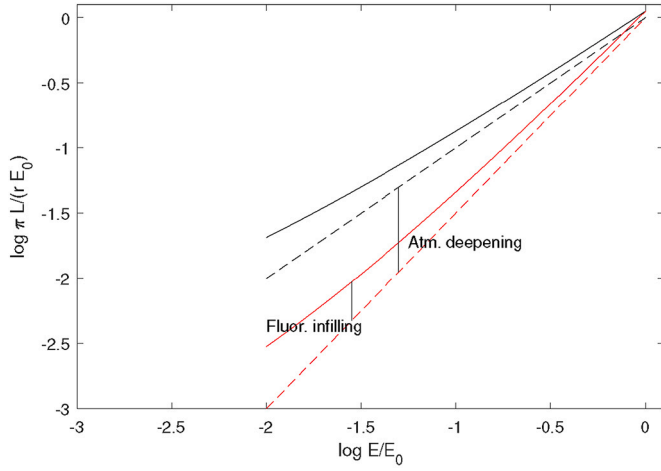The fluorescence contribution makes the relation between $\log \pi L$ and

Fig. 2. Theoretical relations between $\log \pi L/(rE_a)$ versus $\log E/E_a$ for a TOC measurement in absence of fluorescence (dashed black) and in the presence of fluorescence (solid black), and at MH $= 0.25$ atm (at an optical height of 25% of the atmosphere), in absence (dashed red) and in the presence of fluorescence (solid red). The fluorescence contribution is exaggerated to 5% of E_a for illustration purpose.

$\log E$ wavelength dependent. Including SIF (F) to the the upwelling radiance results in:

$$\pi L = \pi(L_r + T_2 F) = E_a r \exp(-k(x_0 + x_1 + x_2)) + \exp(-kx_2)\pi F \quad (5)$$

and thus:

$$\frac{\log \frac{\pi L}{rE_a}}{\log \frac{E}{E_a}} = \frac{\log(\exp(-k(x_0 + x_1 + x_2)) + \pi F/(rE_a)\exp(-kx_2))}{kx_0} \quad (6)$$

As opposed to Eq. (4), the relation in Eq. (6) is wavelength dependent: The wavelength dependent coefficient k cannot be eliminated from the equation. As a consequence, the relation between the enumerator and the denominator in Eq. (6) in the O_2 bands is curved, even for a spectrally constant F. Note that in reality F and E_a are wavelength dependent too, but they change much more gradually and monotonically with wavelength than k. More critical than the spectral shape of E_a and F are the implicit assumption that k is equal over the three paths, and the fact that the convolution with the SRF was ignored in this derivation. Fig. 2 illustrates the expected behaviour of measurements at TOC and MH in the presence and absence of a fluorescence, albeit with an exaggerated and spectrally constant fluorescence contribution for illustration purpose and under the assumptions mentioned above. Fluorescence adds curvature to an otherwise linear relation between $\log L$ and $\log E$.

Theoretically, E_a can be estimated from the Sun-Earth geometry and an ancillary data source of the extraterrestrial radiation, but in practise, it is sufficient to normalize by the shoulders of the O_2 bands, i.e. E_a is estimated from the measured irradiance outside the O_2 bands E_o. Because the atmosphere is not entirely transparent outside the O_2 bands even in cloud-free conditions, mainly due to absorption by aerosols, ozone and water vapour, the atmospheric transmittance T_a outside the O_2 band is not unity. We can separate k into a component due to O_2 absorption alone (k_{O2}) and a component due to other effects (k_{other}):

$$k = k_{O2} + k_{other} \quad (7)$$

where k_{O2} is zero outside the O_2 bands. The effect of k_{other} cancels out when using the following two substitutions derived from the definitions in Fig. 1, into the left hand side of Eq. (4):

$$\log E_a = \log E_o + (k_{other} x_0) \quad (8)$$

$$\log rE_a = \log(L_o - T_2 F) + (k_{other}(x_0 + x_1 + x_2)) \quad (9)$$

such that, after some rearrangement:

$$\frac{\log \frac{L_r}{L_o - T_2 F}}{\log \frac{E}{E_o}} = \frac{x_0 + x_1 + x_2}{x_0} = a \quad (10)$$

In theory, it is now possible to retrieve fluorescence by iteratively removing F from the measured irradiance until the resulting $\log L_r$ in the O_2A band exhibits a linear relationship with $\log E$ according to Eq. (10). However, the earlier mentioned two simplifications, notably ignoring the effects of the the the SRF of the instrument and the assumption that k is identical above and below the measurement height, need further investigation. The convolution partially cancels the (additional) deepening due to the longer path, and this can lead to underestimates in a and F with our approach. The extrapolation of k to the atmosphere below the sensor is critical because the air mass below the sensor typically has a higher temperature and higher pressure than the air mass above. This can lead to differences in the spectral shape between $\log E$ and $\log L$.

3. Methodology

3.1. MODTRAN5 simulations

In order to test the validity of the assumptions of the approach, we used simulations with the atmospheric radiative transfer model MODTRAN5. To ensure realistic input data, we used atmospheric properties obtained from Aeronet sites during clear sky days in Italy, Germany and Spain, at Sentinel-3B overpass times (see github.com/christiaanvandertol/BSF for the input data files) and for one site (Spain), we repeated the simulations for solar zenith angles of 30, 45, 60 and 75 degrees. Simulations with different values of visibility, column water vapour, solar inclination angle, elevation and surface temperature enabled testing of the effects of extrapolation of k and convolution with the SRF.

For four input data files, the surface irradiance was calculated with the T-18 system described by Cogliati et al. (2015) and Verhoef et al. (2018). The simulations were repeated after perturbation of the surface elevation in each of the four MODTRAN5 input data sets, yielding irradiance spectra at a different elevation. This resulted in four pairs of irradiance spectra, each consisting of spectra at two elevations, notably 7 and 81 m, 258 and 324 m, 111 and 125 m, and 69 and 111 m.

The effect of the convolution of with the SRF was investigated and quantified with MODTRAN5 and SCOPE simulated spectra as follows. First, a synthetic 'true' upwelling radiance L in absence of fluorescence was estimated for values of a ranging from 1.0 to 1.1 as:

$$L = \exp(\log(E_{M5} \cdot r) \cdot a) * S_f \quad (11)$$

in which E_{M5} are the high resolution MODTRAN5 direct solar irradiance spectra normalized to the oxygen band shoulders, and r a surface reflectance for green vegetation simulated with SCOPE version 2.1 (default input) (Yang et al., 2021), S_r the spectral response function, for which we used a Gaussian function for each band. In order to study the effect of S_f, we varied the full-width half max (FWHM) from 0.01 to 0.7 nm in steps of 0.01 nm. Second, an equivalent L_{approx} was calculated using convolved solar irradiance as input:

$$L_{approx} = \exp(\log((E_{M5} * S_f) \cdot r) \cdot a), \quad (12)$$

Comparing the two quantities L and L_{approx} allows evaluating the use of the proposed BSF method on measured (convolved) spectra. L and L_{approx} are similar for $a = 1$, but they increasingly diverge as a increases. We found that the difference $L - L_{approx}$ scales with $a - 1$ and the inverse of the cosine of the solar zenith angle (length x_0 in Fig. 1). To correct for the convolution problem, we define a FWHM-dependent correction function (C_{SRF}). The C_{SRF} was calculated by linear regression between

Table 1

Parameters used in the O₂ band shape fitting (BSF) algorithm and in the iFLD method. Note that the iFLD method uses one wavelength in and one out for retrieval of *F*, and wavelength ranges at the shoulders for the interpolation of reflectance. All wavelengths are given in nm.

BSF parameter	value
left boundary (O_2A, O_2B)	759, 686.5
right boundary (O_2A, O_2B)	768, 688.1
reflectance	linearly interpolated over the band
fluorescence O_2A	linear decrease (right $= 0.7*$left)
fluorescence O_2B	uniform
iteration tolerance RMSE	1E-4
max no iterations	30
prior weights of *a* (three scenarios))	10^{12},0,1
iFLD parameters	value
wl,in (O_2A, O_2B)	761,686.9
wl,out (O_2A, O_2B)	755,686.5
left shoulder (O_2A, O_2B)	750–755, 680–685.5
right shoulder (O_2A, O_2B)	772–777, 668.1–690

$(L - L_{approx})/\cos(\theta_s)$ and $(a-1)$ for each wavelength of the instrument (FLoX) in the O₂ bands (see github.com/christiaanvandertol/BSF for the source code). The SRF for the FWHM of 0.31 of the FLoX system ($C_{SRF,FWHM=0.31}$), was archived and further used in the BSF algorithm to correct for the infilling of *L* due the spectral response function as follows:

$$L_c = L + (a - 1) \cdot C_{SRF} \cos(\theta_s) \tag{13}$$

The effect of the extrapolation of *k* was investigated by carrying out linear regression on each of the four pairs (of elevations) of MODTRAN5 simulations. The resulting slope of the regression, which resembles *a*, was compared to the equivalent estimated from the barometric equation (Eq. (17)). The residual of the regression provides insight into spectral differences in *k* in the portion of the atmosphere for which *k* was extrapolated.

3.2. Retrieval algorithm

The fluorescence was retrieved from measurements of *E* and *L* by iterative tuning *F* until $\log(\pi L_r)$, which is $\log\pi(L - F/T_2)$, exhibits the linear relation with $\log(E)$ described by Eq. (10). In other words, the curvature (the deviation from a linear relation due to fluorescence, as in Eq. (10)) was removed from the relationship by subtracting *F* from *L*. The slope of the linear regression between normalised $\log L_r$ and $\log E$ represents the ratio of the optical path lengths to the upwelling and the downwelling radiance measurement ($a = (x_0 + x_1 + x_2)/x_0$). This

quantity *a* can be evaluated by comparing the value obtained by linear regression to theoretical values based on the sun-observer geometry and the measurement height.

The retrieval requires setting a number of parameters, notably the exact definition of the wavelength position of the shoulders of the O₂ bands and the shape of the fluorescence and reflectance over the O₂ bands. The values for these parameters used in this study are summarised in Table 1.

The shape of *F* and *r* over the O₂ absorption features was quantified using simulations with the model SCOPE (Van der Tol et al., 2009; Yang et al., 2021), which showed that a monotonically decreasing function of wavelength to 70% of its value at the right (768 nm) compared to the left shoulder (759 nm) is sufficient to represent the wavelength dependence of *F* over the O₂A band (Appendix A). The O₂B band is located at a peak or plateau of *F* and the local shape varies mostly with the leaf chlorophyll content, with approximately 10% difference between the two shoulders, but no consistent slope. The inconsistent slope is due to variations in foliage chlorophyll content over the season. Because a small slope has little influence on the retrieved SIF values, we used a spectrally constant *F* for the O₂B band.

Finally, the atmospheric transmittance T_2 of *F* over the optical path x_2 was estimated from *a* by using a simplified representation of the illumination-observation geometry. Following the definition sketch in Fig. 1 and neglecting diffuse irradiance by first approximation, x_2 can be expressed as a function of x_1 and the solar zenith angle θ_s and observation viewing angle θ_o as shown in Fig. 1:

$$x_2 = x_1 \frac{\cos\theta_s}{\cos\theta_o} \tag{14}$$

By substitution of $x_0 = \log E/E_a$, $x_2 = \frac{\log T_2}{-k}$ and $x_1 = x_2\frac{\cos\theta_o}{\cos\theta_s}$ in $a = (x_0 + x_1 + x_2)/x_0$, T_2 can be expressed as:

$$\log T_2 = \frac{(a-1)\log\frac{E}{E_o}}{1 + \frac{\cos(\theta_o)}{\cos(\theta_s)}} \tag{15}$$

With these parameters set, the simultaneous retrieval of *a* and *F* from *E* and *L* is carried out in a number of steps to minimise the cost function as in pseudo-code below (Algorithm 1).

Algorithm 1 Retrieve fluorescence

1: Initialisation
2: $x \leftarrow E$ normalised by interpolated E_o (x-axis of linear regression)
3: $y \leftarrow L$ normalised by interpolated L_o (y-axis of linear regression)
4: $a \leftarrow 1$ (initial value)
5: $F \leftarrow 0$ (initial value)
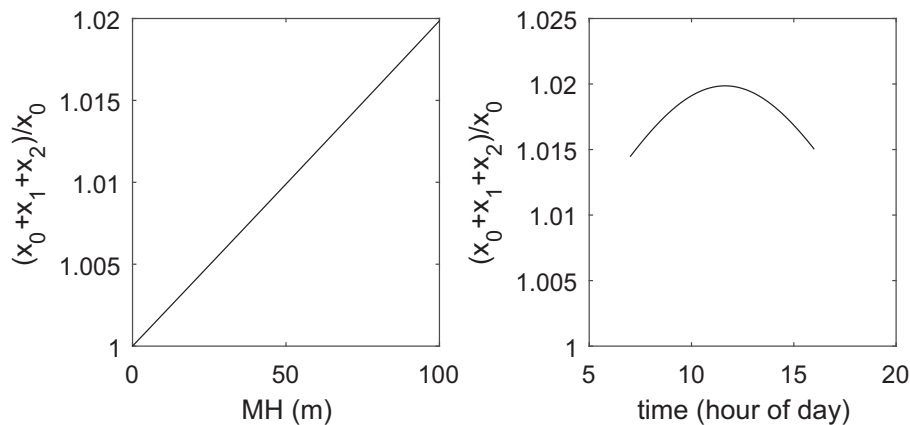6: continue $\leftarrow$ yes

---

Fig. 3. (a) Theoretical relation between sensor height and optical path length *a* at noon (SZA of 44 degrees) assuming adiabatic air pressure profile. (b) theoretical relation between time (with varying solar zenith angle) and optical path length *a* for a sensor height of 100 m at the latitude of the measurement site during solar equinox, assuming adiabatic air pressure profile.
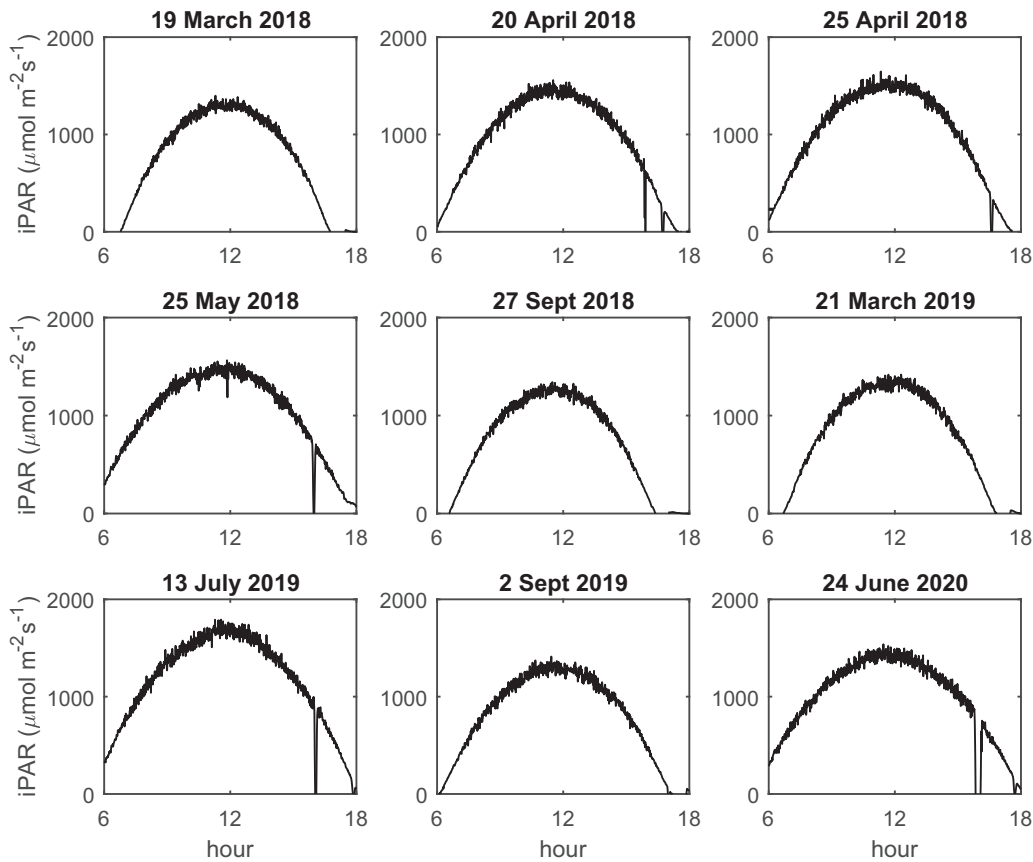
Fig. 4. Incident PAR (400–700 nm) irradiance intensities on the selected days derived from the FLAME spectrometer measurements. Note a shadow effect in the afternoon on days close to northern hemisphere summer solstice.

(*continued*)

```
 7: while continue do
 8:    T₂← Eq. (15): see Eq. (15) for the calculation of this transmittance
 9:    yminF← y −T₂F: Subtract fluorescence
10:    logyminF = log(yminF) - (a-1)*CSRF: take log and apply correction for SRF
11:    a← linreg(x, yminF) apply linear regression
12:    ymod←a*x model log(Lr) from logE with linear regression model
13:    continue ←(ymod −yminF) < threshold (i.e. curvature removed?, see Table 1 for
       stop criteria)
14:    F ← new value chosen towards smaller ymod −y
15: end while
16: Save F and a
```

The following cost function was minimized using a non-linear least square solver, where each update is defined with a Trust Region algorithm:

$$e = \log \frac{\pi L_r}{L_o - F} - a\log \frac{E}{E_o} \tag{16}$$

We used the built-in function 'lsqnonlin' in Matlab 2017a with stopping criteria described in Table 1. As a sanity check, a value for the path length a can be estimated from ratio of pressures at two elevations (p/p_0), assuming optical paths lengths are proportional to air pressure. This ratio can be calculated from p at the MH and p_0 at TOC:

$$p \Big/ p_0 = \frac{x_0}{x_0 + x_1} = \left(1 - \frac{g \cdot z_m}{c_p \cdot T_0}\right)^{c_p \cdot M / R_0} \tag{17}$$

in which $g = 9.81\,\mathrm{m\ s^{-2}}$, molecular mass of air $M = 0.02897\,\mathrm{kg\ mol^{-1}}$, surface temperature T_0, specific heat $c_p = 1004\,\mathrm{J(kg\ K)^{-1}}$, and the gas constant $R_0 = 8.3145\,\mathrm{J(mol\ K)^{-1}}$, and z_m is the MH expressed in metres. In the simulations we used T_0 of 300 K.

Combining this with Eq. (10) leads to a first approximation of a:

$$a = \frac{p_0}{p}\left(1 + \frac{\cos\theta_s}{\cos\theta_o}\right) - \frac{\cos\theta_s}{\cos\theta_o} \tag{18}$$

Examples of this estimate of a as a function of the MH and the solar zenith angle are shown in Fig. 3.

3.3. Evaluation strategy

The approach was evaluated using field data collected with two Fluorescence Box (FLoX) systems (JB Hyperspectral Devices, Düsseldorf, Germany) installed on two towers having different distance from the top of the canopy (namely 100 m and 3 meters) at the experimental site Observatoire de l'Haute Provence (OHP, Saint Michel L'observatoire, France) during an ESA funded FLEX preparatory field campaign (Atmoflex). Because no standard method exists for atmospheric correction and retrieval of reference data of F from the high elevation measurements, a true validation of the approach is not possible. Instead, the algorithm was evaluated indirectly in several steps, which together provide understanding of the sensitivity and accuracy of the approach:

1. **Fluorescence comparison from different elevations**. The retrievals of F at the two elevations were compared to each other. Similar values for F are expected between the two instruments after atmospheric characterisation, because both pieces of equipment were installed in the forest and measured simultaneously. At the lower elevation, atmospheric effects play a minor role. However, due to different footprints of the instruments and due to the heterogeneity of the forest, this comparison cannot be considered as a quantitative validation.
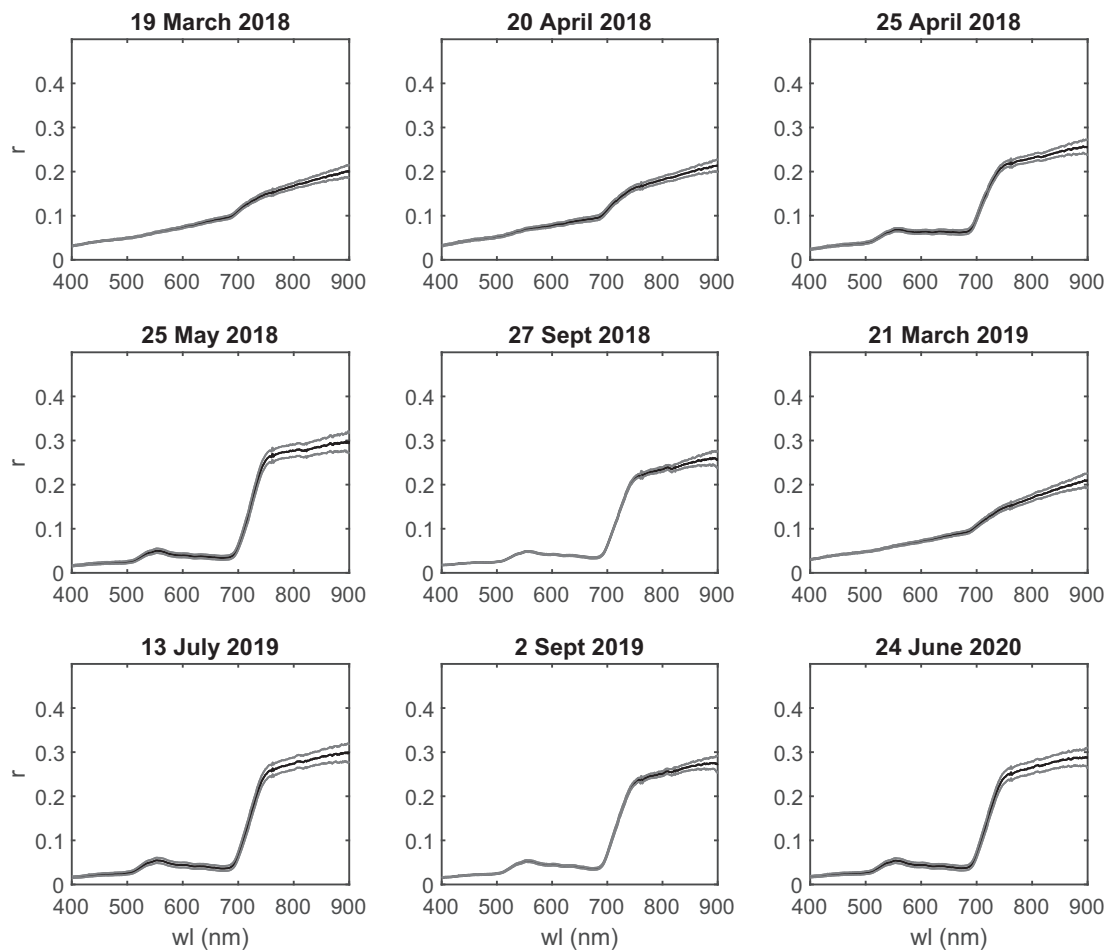
Fig. 5. Daily average apparent (i.e. uncorrected for fluorescence) reflectance spectra for the selected days, and average plus and minus one standard deviation.

2. **Pathlength evaluation**. The retrieved pathlengths serve as a plausibility check: The pathlengths can be approximated by geometrical calculations and the known sensor height. By comparing the retrieved atmospheric path lengths to these values, we can verify whether they agree with expectations based on solar zenith angles and installation heights.

3. **Comparison to model simulated SIF**. The retrieved F is compared to simulations with the model SCOPE. After tuning SCOPE to the measured reflectance, SCOPE is capable of providing realistic values of F both in magnitude and temporal variability (van der Tol et al., 2016).

4. **Comparison to a traditional method**. The proposed retrieval is compared to the established iFLD method (Alonso et al., 2008) for both elevations.

For the benefit of the narrative these evaluations are presented together in a number of figures in the result section, rather than sequential in separate sections.

3.4. Field measurements

The FLoX (Fluorescence BoX) is a field system for high temporal frequency acquisition of continuous TOC radiometric measurements with a focus on SIF (Julitta et al., 2017). The system is equipped with two spectrometers: i) Ocean Insight FLAME S covering the full range of visible and near-infrared (VNIR); and ii) Ocean Insight QEPro with high-spectral resolution (Full Width at Half Maximum – FWHM – of 0.3 nm, SSI 0.15 nm) in the range of the fluorescence emission 650 nm–800 nm.

Each spectrometer's optical input is split into two fiber optics, that lead to i) a cosine receptor measuring the solar irradiance; and ii) a bare fiber measuring the target reflected radiance. Spectrometers are housed in a Peltier thermally regulated box keeping the internal temperature lower than 25°C in order to reduce dark current drift. Moreover, the thermo-electric cooler (TEC) of QEPro is set to 20°C in order to always provide stable measurements. A measurement sequence consists of: i) downwelling radiance, ii) upwelling radiance, iii) a second downwelling radiance, iv) two dark spectra with the same integration time as upwelling and downwelling radiance channels. This is identically repeated for the second spectrometer. The systems were installed at an elevation of 100 m and 3 m above the tree crowns, respectively. The system at 100 m height has been operational for nearly three growing seasons, while the system at 3 m above the crown was operational for less than one month.

A number of clear sky days were selected in the time series at different stages in the annual phenological cycle of the trees (Fig. 4). Note that an obvious shadow effect occurs in the time series in the evening of days close to northern hemisphere summer solstice due to the experimental setup. Furthermore, the reflectance measurements indicate that on a number of days the chlorophyll content was particularly low (19 March 2018 and 21 March 2019), while on other days, the vegetation was dense with high chlorophyll content (e.g. 13 July 2019). Differences in chlorophyll content among days affect the ratio of red: far-red fluorescence. We can expect a higher red: far-red fluorescence ratio on days with low chlorophyll content than on days with a high chlorophyll content. On the 27th of September 2018, both systems (the 100 m high and low installation) were present, allowing a comparison of the
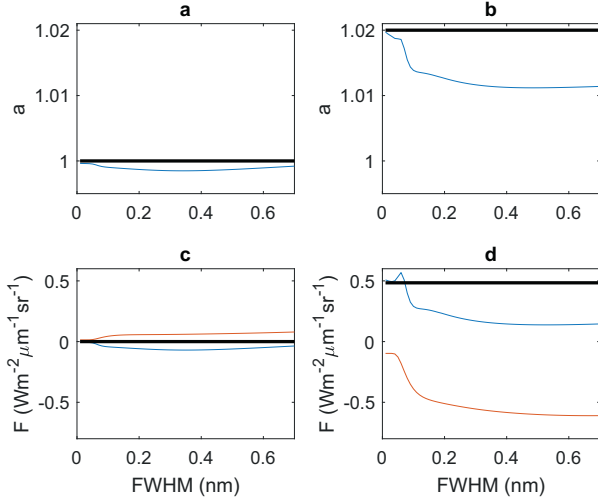
Fig. 6. Retrievals of the optical pathlength a (a,b) and fluorescence (c,d) for synthetic (MODTRAN5) data without (a,c) and with (b,d) fluorescence. The input values were $a = 1$ and $F = 0\,\mathrm{Wm}^{-2}\mu\mathrm{m}^{-1}\mathrm{sr}^{-1}$ (a,c) and $a = 1.02$ $F = 0.5\,\mathrm{Wm}^{-2}\mu\mathrm{m}^{-1}\mathrm{sr}^{-1}$ (b,d). Simulated irradiance spectra in the O$_2$A band were convolved with a Gaussian SRF with a FWHM ranging from 0.01 to 0.70 nm. The black solid lines are the input values, the blue line represents the retrieval with the BSF method, and the red line the retrieval with the iFLD method.

retrievals from two heights at this location.

3.5. SCOPE simulations

Simulations with SCOPE (version SCOPEv2.1 Yang et al. (2021)) were performed for comparison with retrieved fluorescence. The reflectance data of the FLAME spectrometer of the FLoX were used to retrieve leaf optical and canopy structure parameters, including the PROSPECT (Fluspect) parameters, leaf area index, and the leaf inclination distribution parameters LIDFa and LIDFb with the numerical retrieval method described in van der Tol et al. (2016). The retrieved properties were then used in SCOPE to simulate the fluorescence signal in the two O$_2$ bands. The retrieval was carried out once for each of the 10 measurement days, for both the high and low system. For all other inputs, the default values in SCOPE were used. The fluorescence spectra simulated with SCOPE were linearly scaled by the ratio of the total

irradiance measured with the FLAME spectrometer over the total SCOPE irradiance in the corresponding wavelength range. This approach implies that no diurnal variations in fluorescence emission efficiency have been simulated: SCOPE uses the model of Van der Tol et al. (2014) to estimate the photosystem-level emission efficiency, in this case with the default mid-day meteorology, irradiance, and carboxylation capacity as input. In this way the model captures the dominant effects of vegetation structure and irradiance, which are well characterised through the inversion of FLOX reflectance measurements, but not the physiological response, which is not known (see Fig. 5).

4. Results

4.1. Effect of the spectral convolution and extinction extrapolation

Fig. 6 shows that using Eq. (10) with convolved radiances substantially affects the retrieval of fluorescence with the BSF and iFLD methods in the O$_2$A band. Interestingly, this is even the case for measurements at top-of-canopy, TOC (thus: without additional atmospheric deepening). At TOC, we find errors in SIF of about 0.07 W m$^{-2}\mu$m^{-1} sr^{-1} in the iFLD and our BSM method, due to the convolution before the multiplication by r. While this error is small, the problem is more severe at greater heights above the surface. Ignoring the effect of the convolution causes unacceptable errors in retrieved F and a, for example, 50% underestimate of F at a FWHM of 0.31 for $a = 1.02$.

We further investigate the spectral effect of the convolution, notably $\log(L - L_{approx})$ (Fig. 7). The infilling due to the SRF is of similar magnitude as the fluorescence. In the O$_2$B band and for wavelengths beyond 762 nm in the O$_2$A band it even dominates the effect of fluorescence (compare the red to the blue and magenta lines). For a given FWHM, the convolution error appears to scale nearly proportionally to $(a - 1)$ (by approximation) with the inverse of the cosine of θ_s at all wavelengths (Fig. 7c), and this enables a correction as an alternative to a full deconvolution. In the following results, we subtracted $(a - 1)*C_{SRF}/\cos(\theta_s)$ from $\log(L_{norm})$, were C_{SRF} is derived per wavelength as the slope of the relation between $(L - L_{approx})\cos\theta_s$ and $(a - 1)$, i.e. the slope in Fig. 7c. Further analyses (not shown) revealed that the surface reflectance value has limited effect on C_{SRF} and a single FWHM-dependent C_{SRF} spectrum can be used per O$_2$ band.

The correction for the convolution substantially improves the retrieval of a and F from synthetic data (Fig. 8). For a FWHM of 0.31 and input values of a ranging from 1.0 to 1.1, the systematic underestimate of a and F (Fig. 8a,c) vanishes after correction (Fig. 8).
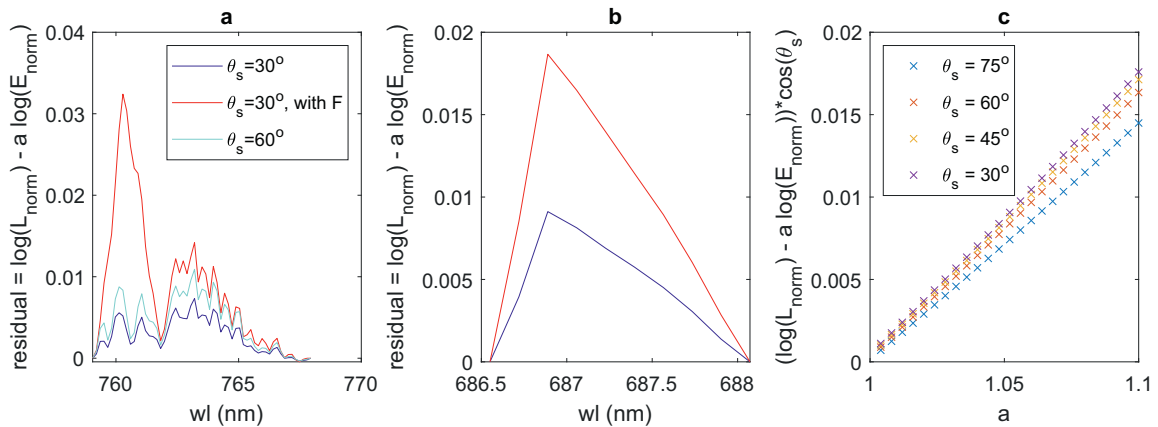

Fig. 7. (a) and (b): The residual of the linear regression of log$L$ versus log$E$, for input values of $a = 1.02$ and FWHM $= 0.31$ nm, where log$L$ was simulated from MODTRAN5 irradiance in the order: first atmospheric propagation, then convolution, for the O$_2$A band (a) and the O$_2$B band (b). Blue and cyan represent L_r i.e. absence of fluorescence, and hence represent $L - L_{approx}$ for two values of θ_s and red $L = L_r + T_2F$ (i.e. including the contribution by SIF). (c): the residual in absence of fluorescence (i.e. $L - L_{approx}$) multiplied by $\cos(\theta_s)$ versus a for a FLoX band at 761 nm for four values of θ_s; the slope is the correction coefficient C_{SRF} at this wavelength.
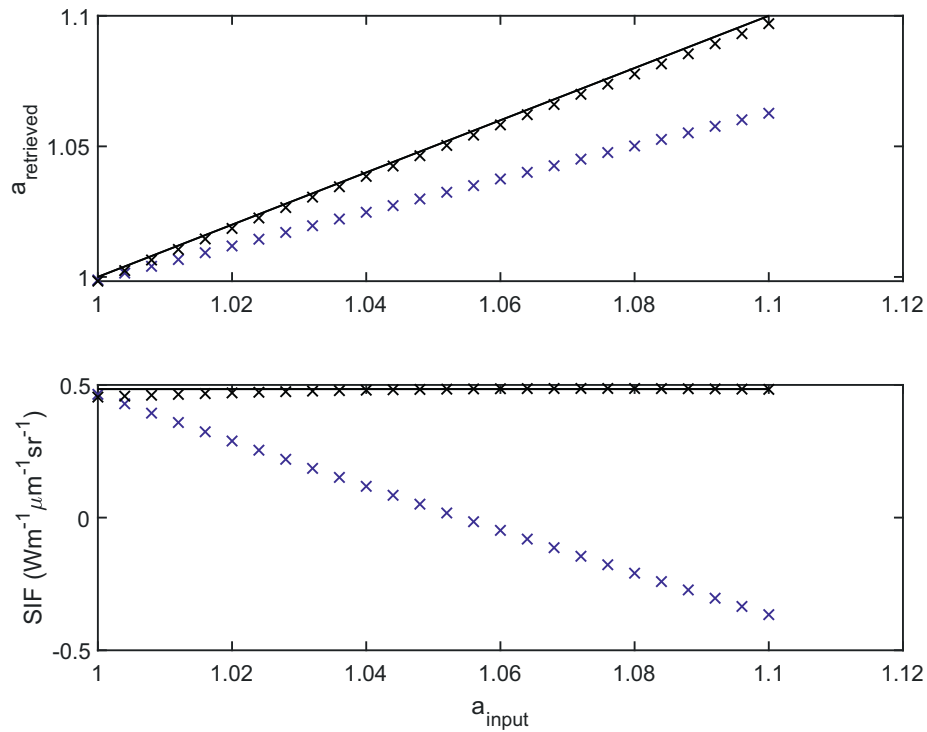
Fig. 8. Retrieval of the optical path length a and fluorescence with Eq. (10), without (blue) and with (black) correction for non-linearity induced by a Gaussian spectral response function of an instrument with a FWHM of 0.3 nm. Input values of a and SIF are shown with bold black lines.
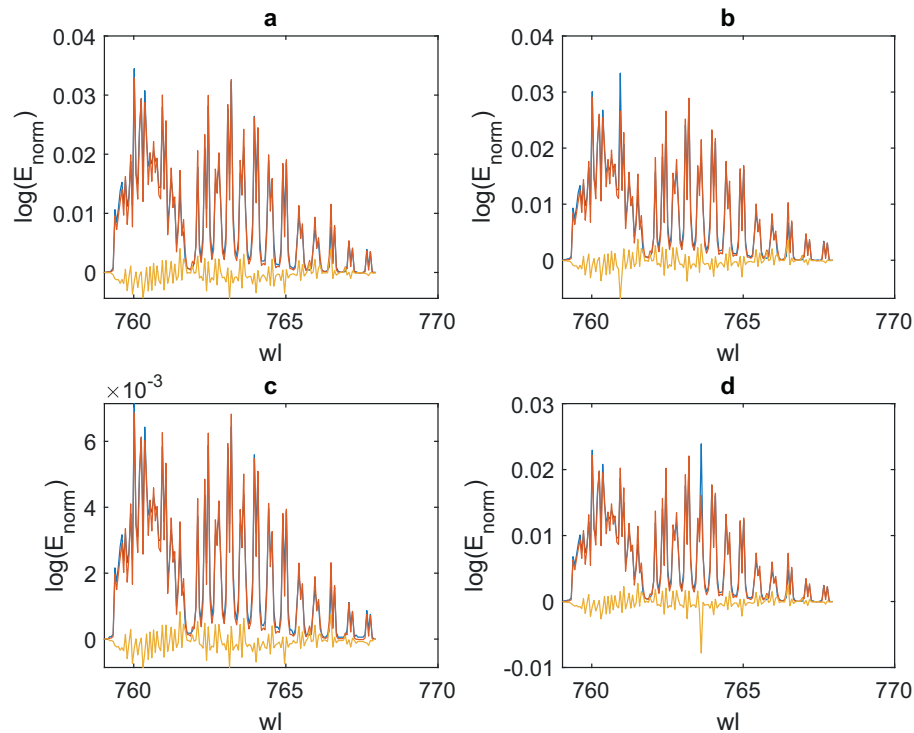

Fig. 9. For four pairs of MODTRAN5 simulations: blue: The difference in $\log E$ as simulated with MODTRAN5; red: The difference between $\log E$ at the greatest height and the $\log E$ extrapolated to the smallest height above the surface with Eq. (10). Yellow: the error in the extrapolation, i.e. the difference between the blue and red curves. Elevations: (a) 7 and 81 m, (b) 258 and 324 m, (c) 111 and 125 m, and (d) 69 and 111 m.

4.2. Validity of the extrapolation of the extinction coefficient

Fig. 9 shows the difference between MODTRAN5 irradiance spectra extrapolated with Eq. (10) by means of linear regression from the highest to the lowest elevation in each simulation pair, and true MODTRAN5 simulations for the lower of the two heights. The residuals of the
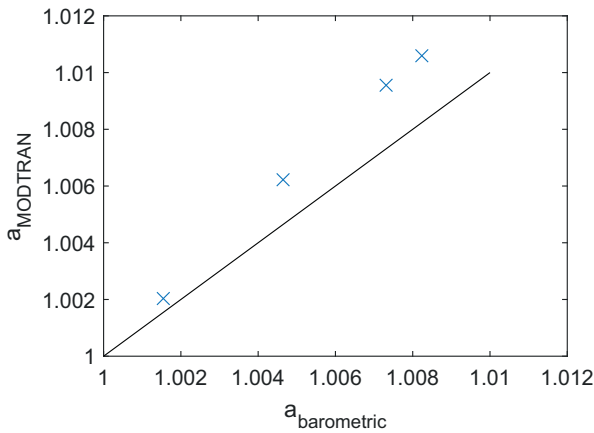
Fig. 10. Values of relative optical depth a retrieved from pairs of MODTRAN5 simulations versus equivalents calculated with the barometric equation for the corresponding four pairs of (input) heights above the surface.
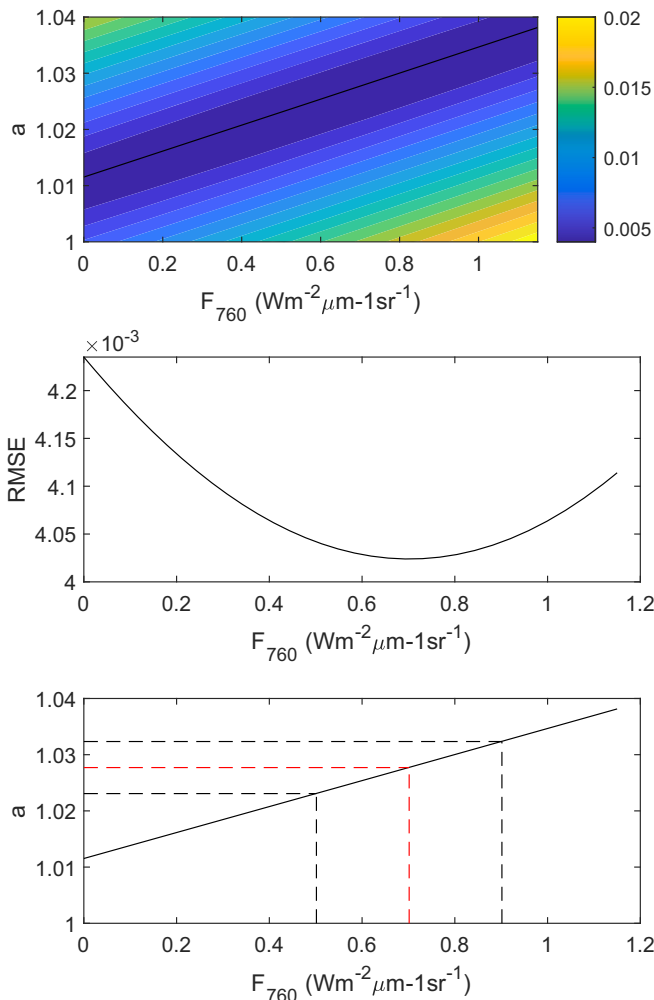

Fig. 11. Top: RMSE of modelled minus measured normalized log $L_r = L - F/T_2$ as a function of F and a, for mid-day of 25 May 2018 at the OHP tower. The black solid line represents the minimum RMSE for each value of F. Middle: The RMSE as a function of F with the relation between F and a as described by the solid line in the upper panel. Bottom: illustration of the relation between a (deepening) and F (infilling): The black dashed lines denote the required accuracy in a for a F accuracy of $0.2\,\mathrm{Wm}^{-2}\mu\mathrm{m}^{-1}\mathrm{sr}^{-1}$.

linear regression represent noise, and these residuals are small compared to the deepening over the height trajectories, and hence, extrapolation is justified. However, the values of a retrieved with linear regression for the four pairs of MODTRAN5 simulations are higher than the barometric equation (Eq. (17)) suggests for the corresponding heights above the surface (Fig. 10).

4.3. Sensitivity analysis for the O2A band

Because the method relies on the separability of infilling by fluorescence and the deepening by oxygen, it is necessary to evaluate whether they are distinguishable in practise. To investigate this, we present the sensitivity of the root mean square error (RMSE) of modelled log-normalized $\pi(L - F/T_2)$ (i.e. the cost function without prior a) to both atmospheric deepening and fluorescence infilling (F). Fig. 11a shows this RMSE for combinations of deepening (y-axis) and infilling (x-axis). The fact that combinations of a and F yield low RMSE indicates that infilling and deepening compensate each other. The presence of a valley of RMSE values along the diagonal of increasing a and F in Fig. 11 illustrates this problem of equifinality. Nevertheless, along the valley (the black line in Fig. 11a), a global minimum in RMSE is present. In this example at an F of $0.70\,\mathrm{Wm}^{-2}\mu\mathrm{m}^{-1}\mathrm{sr}^{-1}$ (Fig. 11b). The presence of a minimum shows that infilling and deepening indeed have spectrally slightly different effects, albeit subtly.

Fig. 11 also shows the sensitivity of fluorescence retrieval to atmospheric characterisation. The 'correct' estimate of a is 1.028 in this case, and the corresponding fluorescence of $0.70\,\mathrm{Wm}^{-2}\mu\mathrm{m}^{-1}\mathrm{sr}^{-1}$ is retrieved (the red dashed line in Fig. 11c). An uncertainty of 0.0036 in a, corresponding to 3.65 hPa at a nominal ambient air pressure (1012 hPa) or +/-17 m in MH leads to an uncertainty in retrieved F of $0.2\,\mathrm{Wm}^{-2}\mu\mathrm{m}^{-1}\mathrm{sr}^{-1}$ (dashed lines in Fig. 11c).

4.4. Fluorescence comparison between elevations and methods

Fig. 12 shows measurements of E and L over the O$_2$A band for noon of 27 September 2019, for the FLoX systems installed at both heights: 3 m from the canopy (top panels) and at 100 m height (bottom panels). In the first case, the normalised radiance (triangles) is slightly higher than the irradiance (circles) due to fluorescence infilling. The normalised upwelling radiance plotted versus the normalised irradiance fall just above the 1:1 line (black circles in Fig. 12b). When the fluorescence is subtracted, the relation between L_r and E collapses onto the 1:1 line. However, for measurements at 100 m height (lower panels, Fig. 12c and d), the infilling is fully compensated by additional deepening, such that the normalised L and E are nearly on the 1:1 line (black circles in Fig. 12c and d), and only a subtle curvature of the relationship remains. Removing the curvature by subtracting F then lowers $\log L_r$ below $\log E$. The resulting linear relation has a slope a of 1.026 (red dashed line and triangles), which represents the ratio of the optical path lengths of L and E.

Fig. 13 shows the results for the O$_2$B band for the same measurements as Fig. 12. Note that the absorption feature is less deep than the O$_2$A feature, hence both the high and low elevation show infilling in L compared to E. We did not retrieve the path lengths a from the O$_2$B band again, but used the values retrieved earlier from the stronger O$_2$A feature, in other words, fluorescence in the O$_2$B band was retrieved with a known atmosphere.

We further compared the retrieved fluorescence from two heights for a full diurnal cycle (27 September 2018) in both oxygen bands, and investigated the retrieval of F without ($a = 1$) and with (a retrieved) atmospheric correction, for both systems. Fig. 14 confirms our expectation that without atmospheric correction, there is a large difference between the retrieved fluorescence in the O$_2$A band between the two elevations, where retrievals from the high elevation yield unrealistically low and even negative fluorescence values.
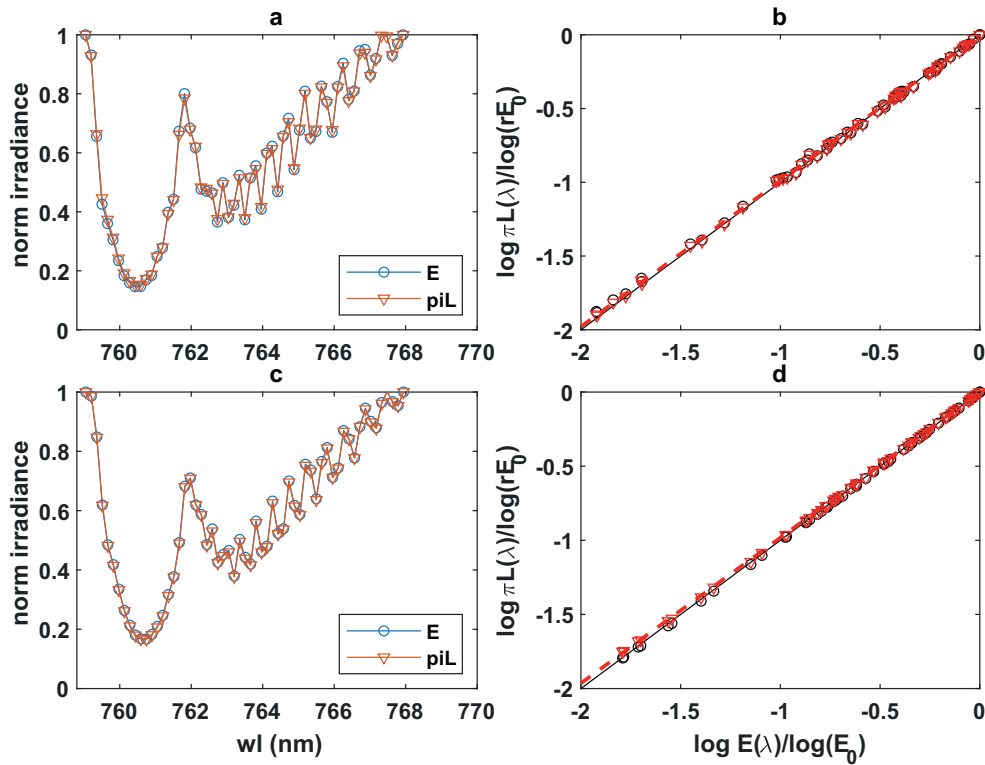
Fig. 12. (a) Measured normalised (to absorption band edges) solar irradiance E and upwelling radiance L over the O$_2$A feature for the low altitude system; (b) normalised L versus normalised E for the O$_2$A feature (black circles), normalised L_r versus normalised E for the O$_2$A feature (red triangles), the 1:1 line (solid black) and linear regression through L_r versus E (red dashed). The slope of the red dashed line represents the retrieved a. (c) and (d): idem, but for the high altitude system.
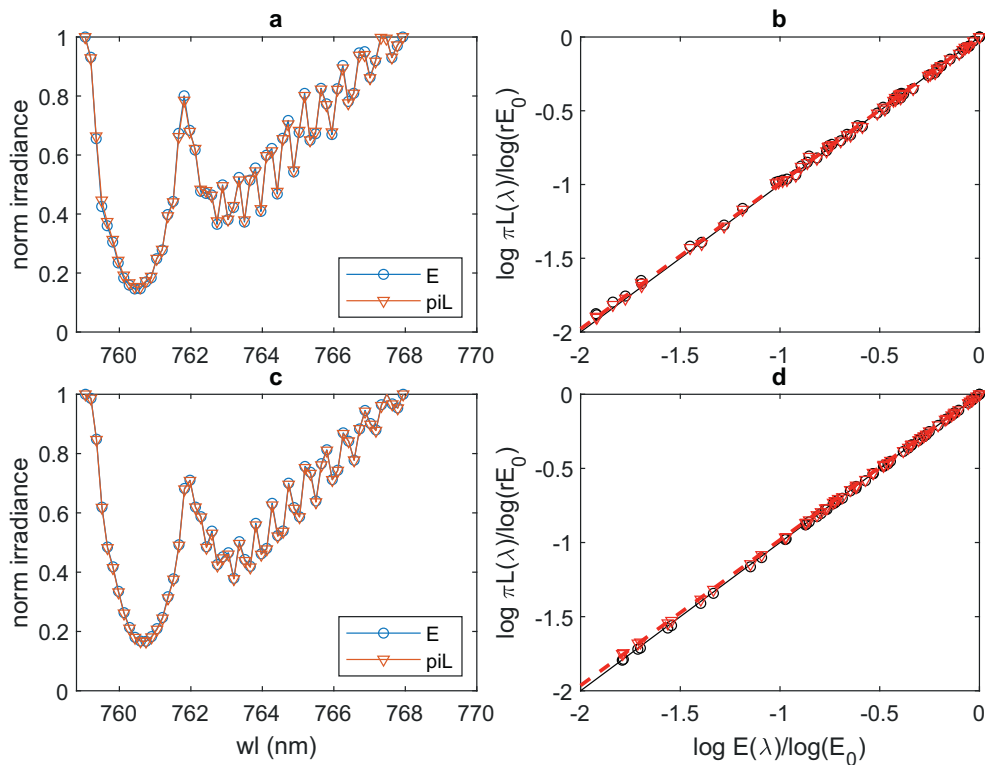

Fig. 13. (a) Measured normalized (to absorption band edges) solar irradiance E and upwelling radiance L over the O$_2$B feature for the low altitude system; (b) normalized L versus normalized E for the O$_2$B feature (black circles), normalized Lr versus normalized E for the O$_2$B feature (red triangles), the 1:1 line (solid black) and $a \cdot E$ (red dashed), where a was retrieved from the O$_2$A band. (c) and (d): idem, but for the high altitude system.
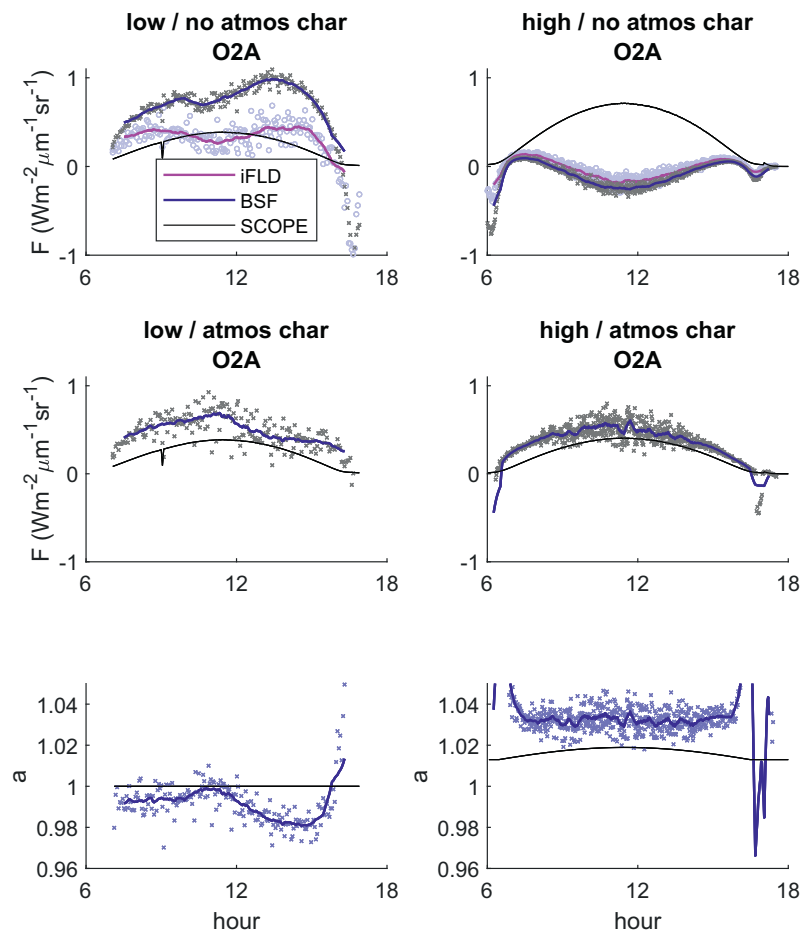
Fig. 14. (a) Retrieved fluorescence in the O_2A band with BSF (dark gray symbols) and moving average (blue line), along with iFLD (light gray and purple) and SCOPE simulated fluorescence for 27 August 2018 (black line), for the low altitude system with no atmospheric characterization; (b) as (a) but for the high altitude system; (c) and (d) as (a) and (b) but with atmospheric characterization; (e) and (f) retrieved atmospheric path length a for the low and high altitude system, respectively, along with the theoretical values based on altitude and solar inclination (fine line).
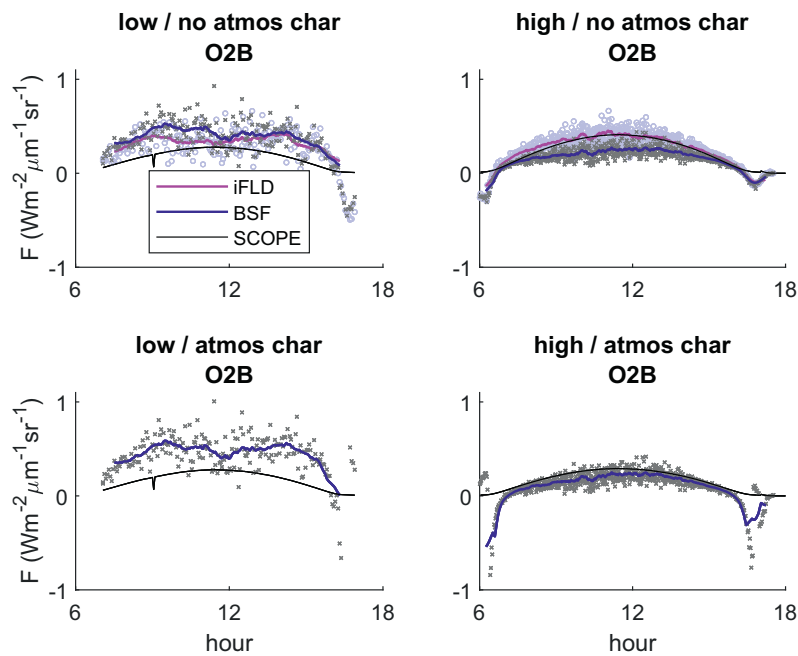

Fig. 15. (a) Retrieved fluorescence in the O_2B band with BSF (dark gray symbols) and moving average (blue line), along with iFLD (light gray and purple) and SCOPE simulated fluorescence for 27 August 2018 (black line), for the low altitude system with no atmospheric characterization; (b) as (a) but for the high altitude system; (c) and (d) as (a) and (b) but with atmospheric characterization retrieved from the O_2A band.
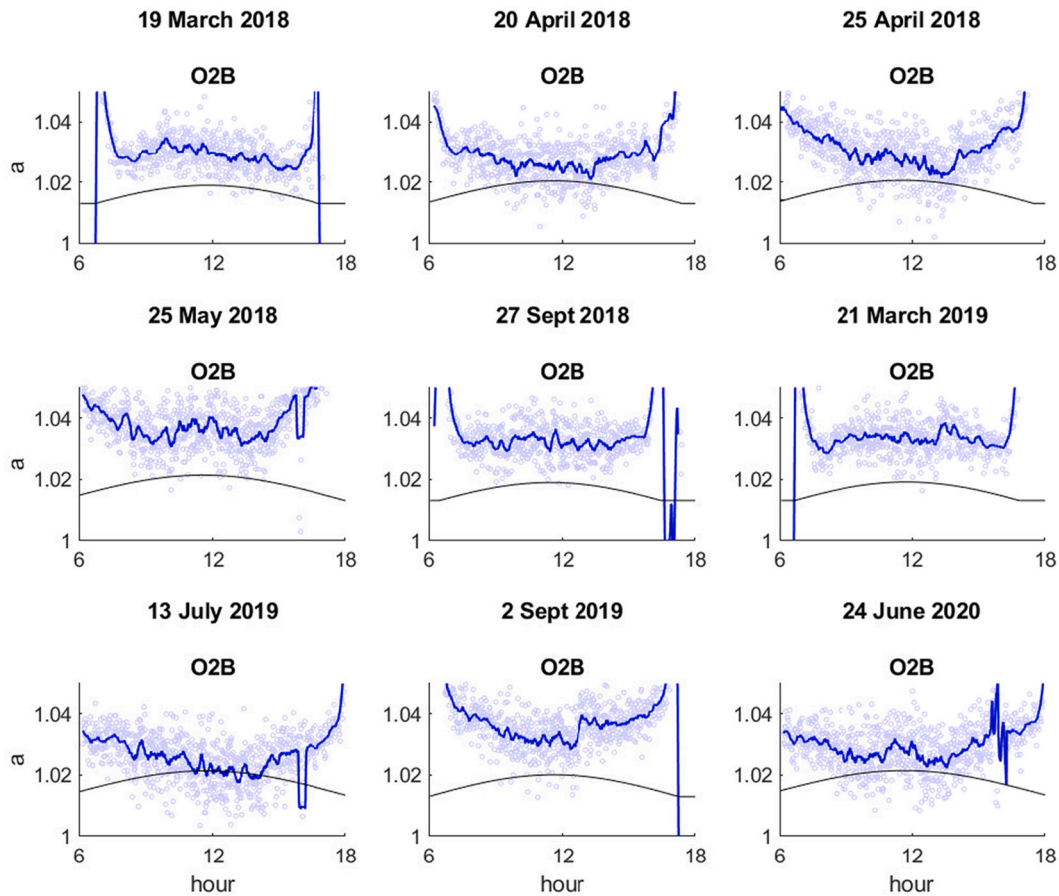
Fig. 16. (a) Retrieved (from the O_2A band infilling) atmospheric optical path lengths a for nine selected days. The lines represent 20 measurement point moving averages (approximately half-hour intervals).

For comparison, SCOPE simulated values and the retrievals with the iFLD method (uncorrected for the atmosphere) are presented as well. For the O_2A band, the BSF method provides higher values than both iFLD and SCOPE at the low elevation, but the diurnal shape of BSF and iFLD retrievals are similar, both showing a late morning depression and negative values in the late afternoon.

Atmospheric correction results in realistic and positive values of fluorescence at both elevations that agree with each other, and with SCOPE simulations (the fine solid line), albeit with an overestimate of retrieved fluorescence compared to SCOPE in the low elevation case.

Interestingly, not only the retrievals from the higher elevation system, but also that of the lower elevation are affected by atmospheric characterisation. The shape of the diurnal cycle of retrieved fluorescence is more realistic after atmospheric correction and in agreement with SCOPE, and negative values disappear. Instead, the retrieved optical path length a shows variation over time. The retrieved values of a for the lower altitude measurements are below unity. This is counter-intuitive, because it suggests a shorter atmospheric path length for the reflected than for the incoming radiation. A possible explanation is directional reflectance. The depths of the O_2 bands may differ between direct and diffuse radiation, and if the corresponding reflectances also differ, then the infilling in L may deviate from that in E. Another possible explanation is that the different foreoptics for the reflected radiation and the incident radiation caused different straylight between L and E, but we found no evidence that this was the case during the calibration of the instrument. For the measurement at the higher elevation, we find values of a around 1.03, higher than the theoretical value based on the barometric equation and the solar inclination angle (thin solid line). The overestimate of a compared to the barometric equation is consistent with the findings for the synthetic data, indicating that air pressure

alone is insufficient to model the additional deepening. During the hours close to sunrise and sunset, retrieved a reached unrealistically high values. We suspect that either a strong increase in the fraction of diffuse radiation, or a known issue with the specific cosine receptor that was used in this FLoX system (CC Oplance glass receptor, Ocean Optics) is responsible. In later versions and upgrades of the FLoX, the cosine receptor has been replaced by a different model. The low altitude system exhibits a similar problem close to sunset, which, if not accounted for by atmospheric characterisation, leads to negative fluorescence values as well. Until this is resolved, the retrievals at low solar altitudes need to be interpreted with care.

Overall the joint atmospheric characterisation and fluorescence retrieval leads to realistic values for each: the retrieved atmospheric path lengths agree with the expected value based on altitude, and the retrieved fluorescence values at the two altitudes agree with each other and with SCOPE simulations.

Fig. 15 shows the same cases, but for the O_2B band. For this band, the effect of atmospheric deepening is substantially less, but we nevertheless observe an improvement in the retrieved fluorescence for both the low and the high altitude system after accounting for the deepening. Atmospheric characterisation improves the agreement between red fluorescence retrieved at the two elevations, the correspondence with SCOPE simulations, and it removes negative fluorescence values close to sunset.

4.5. Evaluations for multiple days in the season

We further evaluate the performance of the retrieval algorithm for the tall tower of both a and F for clear sky days in different moments in the growing season (Figs. 16–18). The retrieved a (Fig. 16) is
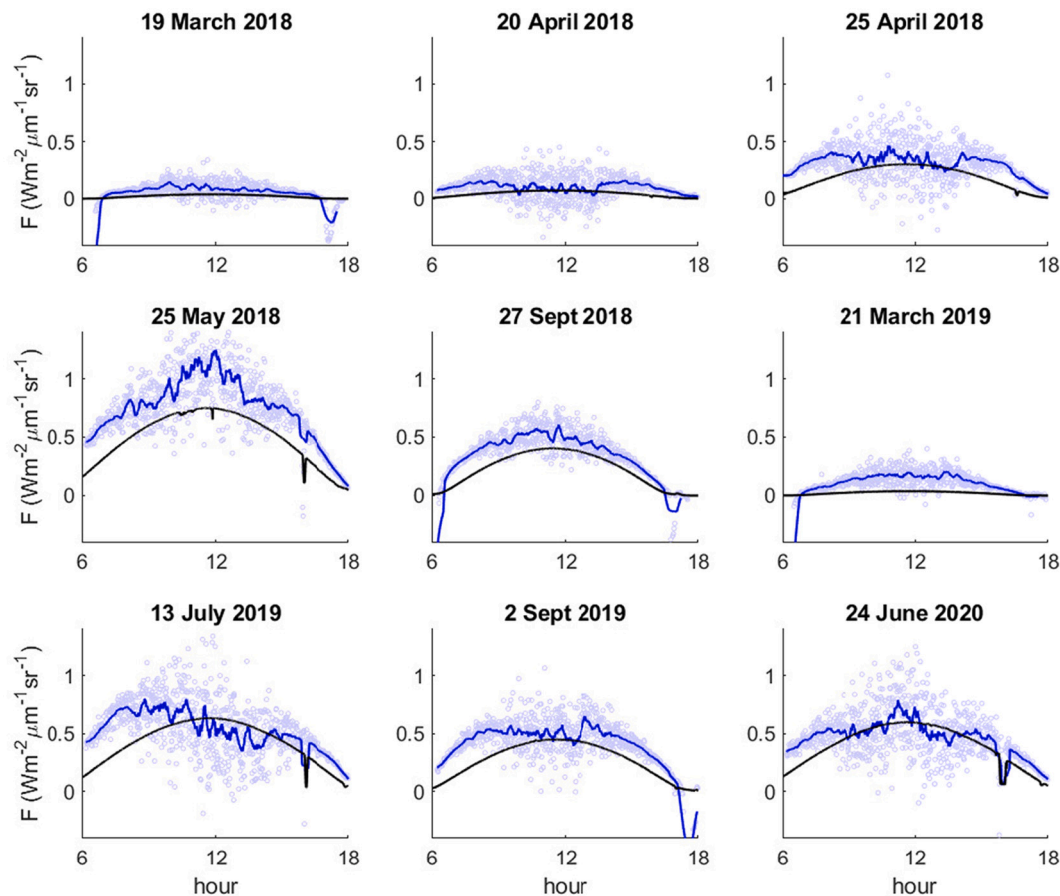
Fig. 17. (a) Retrieved fluorescence from measurements at the highest elevation in the O_2A band along with SCOPE simulated fluorescence for 9 example days.

consistently higher than the value calculated based on the barometric equation. This finding is consistent with Fig. 10.

The retrieval of F in the O_2A band follows SCOPE simulations to some degree (Fig. 17). The diurnal pattern in SCOPE simulated SIF, which is due to the irradiance intensity, and the seasonal variability, which is due to pigment and canopy properties, are both reproduced. To some degree, diurnal differences in fluorescence emission efficiency may explain discrepancies in SIF values between SCOPE and the retrievals, in particular the mid-day depressions in July and September 2019. The retrievals close to sunrise and sunset may suffer from measurement error under low solar angles.

For the O_2B retrievals, we observe reasonable agreement with SCOPE simulations as well, but values were around zero on both days in March (2018 and 2019), and underestimated in April 2018. It should be noted that the effect of the SRF on the O_2B band was substantial, and the simple correction my not suffice for retrievals of such low fluorescence values as in March.

5. Discussion

In this study we proposed to use information in the spectral shape of the observed radiances over the O_2 bands to separate infilling from deepening as an alternative to explicit modelling of the deepening. This is approach fundamentally different from some other FLD methods, such as iFLD (Alonso et al., 2008), in which single wavelengths are selected for within and outside the absorption feature. In our approach, all measurements that are present in the absorption feature contribute to (and are needed for) the separation of infilling from deepening.

The approach is also different from some contemporary spectral fitting methods (SFM) such as the one proposed by Cogliati et al. (2015; Cogliati et al., 2019 which uses the top-of-canopy (TOC) apparent reflectance spectra, and does not accommodate for additional atmospheric deepening. In contrast, in the present study we consider the shape of the O_2 feature as influenced by both the atmosphere and the fluorescence. The fitting is limited to the O_2 bands, hence a much narrower range in which the spectral shape of R and F is less relevant. In contrast, the shape of the absorption band itself is exploited to separate atmospheric deepening from fluorescence infilling. In principle, spectral fitting methods over a wider spectral range are also capable of using this information, provided that atmospheric characterisation and fluorescence retrieval are carried out together and not sequential. Satellite remote sensing retrieval algorithms aiming at a SIF data product avoid the O_2 bands, and focus on spectral windows that are free of significant atmospheric absorption but contain solar absorption features (Köhler et al., 2015; Bacour et al., 2021; Guanter et al., 2021; Sun et al., 2018). Full-spectrum retrieval algorithms aiming at XCO_2 include the O_2A band and also use fluorescence spectra as state variable, but in these retrievals strong priors derived from narrow SFL are used for the fluorescence magnitude, to avoid errors due to the atmosphere propagating into the fluorescence (Taylor et al., 2020).

The finding that deepening and infilling are separable raises the question whether a similar method may be applied to airborne or satellite retrievals in the O_2 bands as well. Airborne measurements follow a different measurement scheme than the tall tower setup in Fig. 1. For example, in the retrieval from Hyplant observations (Rascher et al., 2015), the irradiance is computed as $\pi L/r$ of non-fluorescence surfaces in the vicinity of the target, rather than measured with a cosine receptor. Because such references will most likely not share the atmospheric properties with the vegetation targets due to topography or spatial differences in atmospheric properties and flight altitude, differences in the
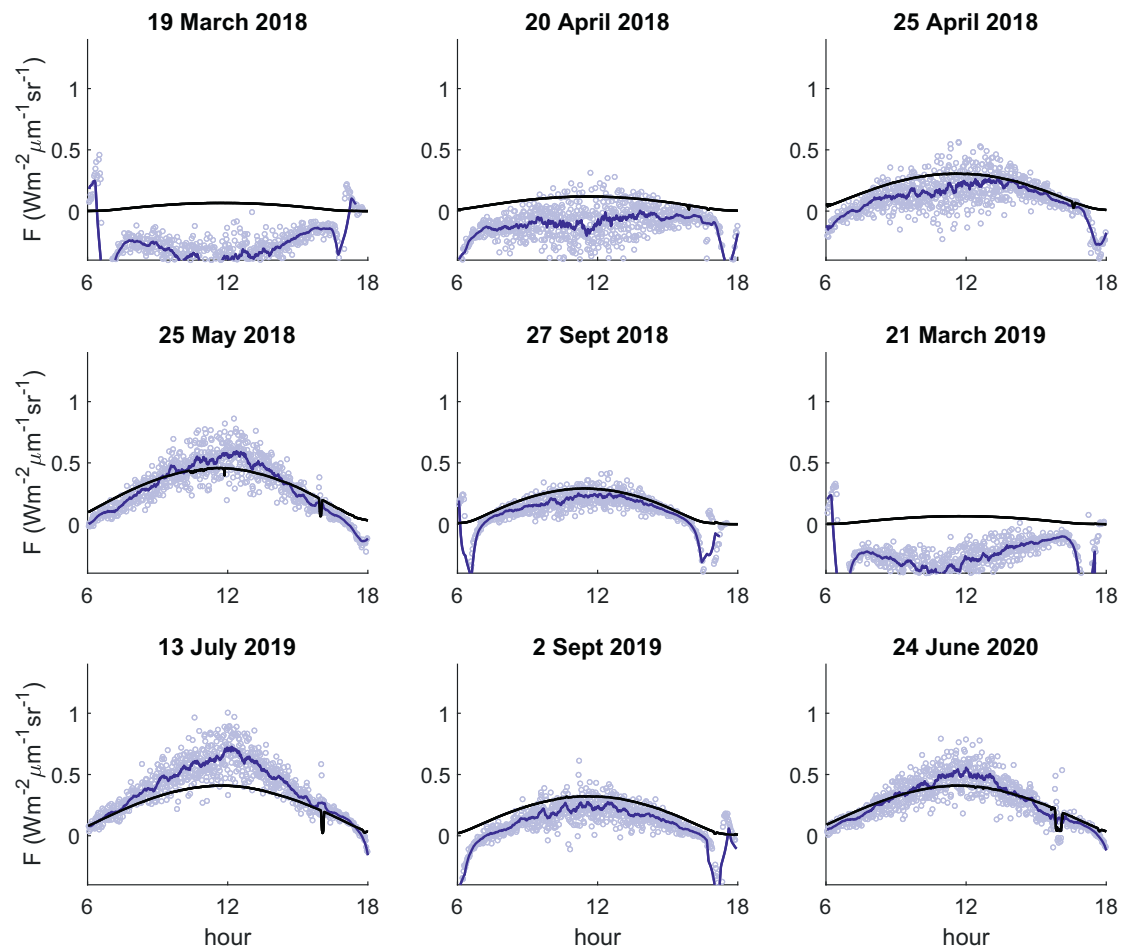
Fig. 18. (a) Retrieved fluorescence from measurements at the highest elevation in the O$_2$B band along with SCOPE simulated fluorescence for 9 example days. The lines represent 20 measurement point moving averages (approximately half-hour intervals), and the solid black line the SCOPE simulation.

depth of the O$_2$ band may arise that are unrelated to SIF. Band shape fitting of the O$_2$ band may then possibly help to correct for differences in optical paths between E (obtained from non-fluorescence targets) and L (vegetated) measurements and at the same time aid the retrieval of F if the infilling and deepening is spectrally different.

However, our study also shows that the retrieval of fluorescence in the O$_2$ band is highly sensitive to the atmosphere and the spectral response function of the instrument. The BSF method appears effective for tall tower measurements, and the possibility to correct airborne retrieval algorithms for small differences in atmospheric composition in a flight line may be further investigated. We do not expect the BSF method to work for airborne FLoX systems or satellite data. Multiple confounding factors, such as the SRF of the instrument, will start to dominate the effect of fluorescence on the shape of the O$_2$ features as the MH increases. In addition, the effect of path radiance (radiance originating from out-of-view, due to scattering by the atmosphere towards the sensor) becomes more prominent. Path radiance effectively means that L is a superposition of contributions with different O$_2$ band depths. Adding these terms to Eq. (10) leads to further curvature of the relation between log$E$ and log$L$.

6. Conclusions

We presented an approach to simultaneously retrieve relative atmospheric path lengths and fluorescence. The information to separate fluorescence infilling from atmospheric deepening originates from the spectral shape of the O$_2$A band. The joint retrieval of atmospheric op-

tical path and fluorescence is useful if the optical path lengths cannot be known accurately, for example if uncertainty exists in the distance to target due to multiple scattering (forest) or if atmospheric conditions vary during the measurements. Evaluation using simulated data (MODTRAN and SCOPE) and a comparison between retrievals at two heights show the BSF method yields plausible values for the atmospheric path length and the fluorescence from tall towers.

Author responsibilities

CvdT conceived and developed the ideas and wrote the code and most of the paper. TJ developed the instruments, the measurement protocol, and the field data processing protocols. TJ, IJ, MT, DS designed the experiments. PY coded the iFLD retrieval algorithm based on the literature. All authors contributed to the writing and refinement of the approach.
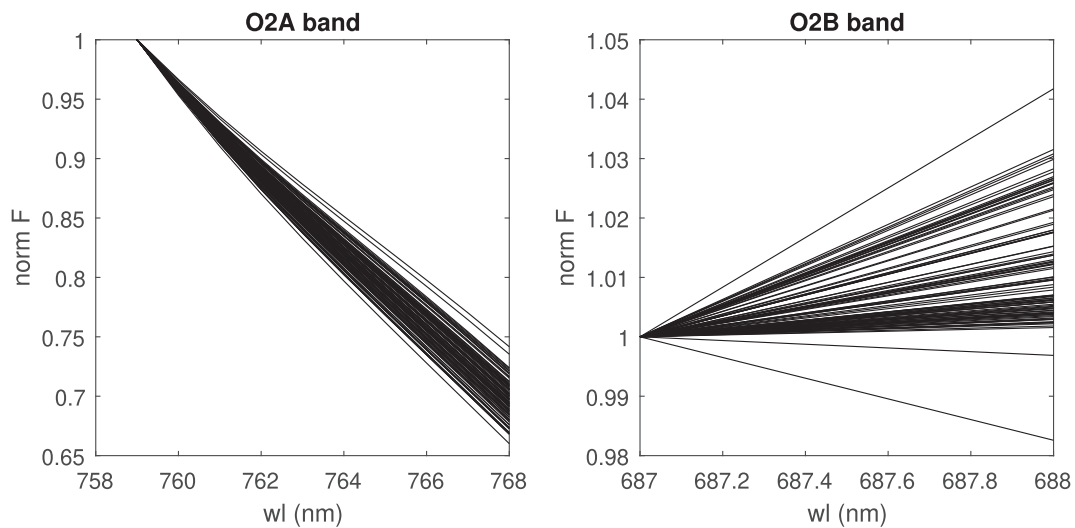
Fig. A.19. Fluorescence in the O_2A and O_2B band normalized by their values at the left shoulder, as simulated with SCOPE for 100 cases with input data sampled over the entire input space using Latin hypercube sampling.

Data availability

Code will be published on https://github.com/christiaanvandertol, and if the paper is accepted, in a stable respository

Acknowledgement

Appendix A. SCOPE fluorescence spectral shapes

The spectral shape of fluorescence over the O_2 bands was investigated using 100 SCOPE simulations with input selected with a Latin hypercube sampling over the entire input parameter space. Fig. A.19 shows the results for both O_2 bands.

References

Aasen, H., Van Wittenberghe, S., Sabater Medina, N., Damm, A., Goulas, Y., Wieneke, S., Hueni, A., Malenovskỳ, Z., Alonso, L., Pacheco-Labrador, J., et al., 2019. Sun-induced chlorophyll fluorescence ii: review of passive measurement setups, protocols, and their application at the leaf to canopy level. Remote Sens. 11 (8), 927.

Alonso, L., Gomez-Chova, L., Vila-Frances, J., Amoros-Lopez, J., Guanter, L., Calpe, J., Moreno, J., 2008. Improved fraunhofer line discrimination method for vegetation fluorescence quantification. IEEE Geosci. Remote Sens. Lett. 5 (4), 620–624.

Bacour, C., Guanter, L., Schneider, A., Aben, I., Maignan, F., Grignon, L., El Hajj, M., Retscher, C., 2021. A new sif (solar induced chlorophyll fluorescence) product derived from tropomi onboard sentinel-5 precursor. En: EGU General Assembly Conference Abstracts. pp. EGU21–8420.

Cendrero-Mateo, M.P., Wieneke, S., Damm, A., Alonso, L., Pinto, F., Moreno, J., Guanter, L., Celesti, M., Rossini, M., Sabater, N., et al., 2019. Sun-induced chlorophyll fluorescence iii: benchmarking retrieval methods and sensor characteristics for proximal sensing. Remote Sens. 11 (8), 962.

Cogliati, S., Celesti, M., Cesana, I., Miglietta, F., Genesio, L., Julitta, T., Schuettemeyer, D., Drusch, M., Rascher, U., Jurado, P., et al., 2019. A spectral fitting algorithm to retrieve the fluorescence spectrum from canopy radiance. Remote Sens. 11 (16), 1840.

Cogliati, S., Verhoef, W., Kraft, S., Sabater, N., Alonso, L., Vicent, J., Moreno, J., Drusch, M., Colombo, R., 2015. Retrieval of sun-induced fluorescence using advanced spectral fitting methods. Remote Sens. Environ. 169, 344–357.

Damm, A., Erler, A., Hillen, W., Meroni, M., Schaepman, M.E., Verhoef, W., Rascher, U., 2011. Modeling the impact of spectral sensor configurations on the fld retrieval accuracy of sun-induced chlorophyll fluorescence. Remote Sens. Environ. 115 (8), 1882–1892.

Frankenberg, C., Butz, A., Toon, G., 2011. Disentangling chlorophyll fluorescence from atmospheric scattering effects in o2 a-band spectra of reflected sun-light. Geophys. Res. Lett. 38 (3).

Grossmann, K., Frankenberg, C., Magney, T.S., Hurlock, S.C., Seibt, U., Stutz, J., 2018. Photospec: a new instrument to measure spatially distributed red and far-red solar-induced chlorophyll fluorescence. Remote Sens. Environ. 216, 311–327.

Guanter, L., Alonso, L., Gómez-Chova, L., Meroni, M., Preusker, R., Fischer, J., Moreno, J., 2010. Developments for vegetation fluorescence retrieval from spaceborne high-resolution spectrometry in the o2-a and o2-b absorption bands. J. Geophys. Res.: Atmos. 115 (D19).

Guanter, L., Bacour, C., Schneider, A., Aben, I., van Kempen, T.A., Maignan, F., Retscher, C., Köhler, P., Frankenberg, C., Joiner, J., et al., 2021. The troposif global sun-induced fluorescence dataset from the sentinel-5p tropomi mission. Earth Syst. Sci. Data Discuss. 1–27.

Julitta, T., Burkart, A., Rossini, M., Schickling, A., Colombo, R., Rascher, U., Cogliati, S., Migliavacca, M., 2017. Flox: a system for automatic long term measurements of top of canopy sun induced chlorophyll fluorescence. En: FLEX 2017 Workshop, ESA-ESRIN. ESA: FLEX.

Köhler, P., Frankenberg, C., Magney, T.S., Guanter, L., Joiner, J., Landgraf, J., 2018. Global retrievals of solar-induced chlorophyll fluorescence with tropomi: First results and intersensor comparison to oco-2. Geophys. Res. Lett. 45 (19), 10–456.

Köhler, P., Guanter, L., Joiner, J., 2015. A linear method for the retrieval of sun-induced chlorophyll fluorescence from gome-2 and sciamachy data. Atmos. Meas. Tech. 8 (6), 2589–2608.

Liu, X., Guo, J., Hu, J., Liu, L., 2019. Atmospheric correction for tower-based solar-induced chlorophyll fluorescence observations at o2-a band. Remote Sens. 11 (3), 355.

Marrs, J.K., Jones, T.S., Allen, D.W., Hutyra, L.R., 2021. Instrumentation sensitivities for tower-based solar-induced fluorescence measurements. Remote Sens. Environ. 259, 112413.

Mohammed, G.H., Colombo, R., Middleton, E.M., Rascher, U., van der Tol, C., Nedbal, L., Goulas, Y., Pérez-Priego, O., Damm, A., Meroni, M., et al., 2019. Remote sensing of solar-induced chlorophyll fluorescence (sif) in vegetation: 50 years of progress. Remote Sens. Environ. 231, 111177.

Rascher, U., Alonso, L., Burkart, A., Cilia, C., Cogliati, S., Colombo, R., Damm, A., Drusch, M., Guanter, L., Hanus, J., et al., 2015. Sun-induced fluorescence–a new probe of photosynthesis: first maps from the imaging spectrometer hyplant. Glob. Change Biol. 21 (12), 4673–4684.

Sabater, N., Kolmonen, P., Van Wittenberghe, S., Arola, A., Moreno, J., 2021. Challenges in the atmospheric characterization for the retrieval of spectrally resolved fluorescence and pri region dynamics from space. Remote Sens. Environ. 254, 112226.

Sabater, N., Vicent, J., Alonso, L., Verrelst, J., Middleton, E.M., Porcar-Castell, A., Moreno, J., 2018. Compensation of oxygen transmittance effects for proximal sensing retrieval of canopy–leaving sun–induced chlorophyll fluorescence. Remote Sens. 10 (10), 1551.

Sun, Y., Frankenberg, C., Jung, M., Joiner, J., Guanter, L., Köhler, P., Magney, T., 2018. Overview of solar-induced chlorophyll fluorescence (sif) from the orbiting carbon

observatory-2: retrieval, cross-mission comparison, and global monitoring for gpp. Remote Sens. Environ. 209, 808–823.

Taylor, T.E., Eldering, A., Merrelli, A., Kiel, M., Somkuti, P., Cheng, C., Rosenberg, R., Fisher, B., Crisp, D., Basilio, R., et al., 2020. Oco-3 early mission operations and initial (yearly) xco2 and sif retrievals. Remote Sens. Environ. 251, 112032.

Van der Tol, C., Berry, J., Campbell, P., Rascher, U., 2014. Models of fluorescence and photosynthesis for interpreting measurements of solar-induced chlorophyll fluorescence. J. Geophys. Res.: Biogeosci. 119 (12), 2312–2327.

van der Tol, C., Rossini, M., Cogliati, S., Verhoef, W., Colombo, R., Rascher, U., Mohammed, G., 2016. A model and measurement comparison of diurnal cycles of sun-induced chlorophyll fluorescence of crops. Remote Sens. Environ. 186, 663–677.

Van der Tol, C., Verhoef, W., Timmermans, J., Verhoef, A., Su, Z., 2009. An integrated model of soil-canopy spectral radiances, photosynthesis, fluorescence, temperature and energy balance. Biogeosciences 6 (12).

Verhoef, W., Van Der Tol, C., Middleton, E.M., 2018. Hyperspectral radiative transfer modeling to explore the combined retrieval of biophysical parameters and canopy fluorescence from flex–sentinel-3 tandem mission multi-sensor data. Remote Sens. Environ. 204, 942–963.

Yang, P., Prikaziuk, E., Verhoef, W., van der Tol, C., 2021. Scope 2.0: A model to simulate vegetated land surface fluxes and satellite signals. Geosci. Model Dev. 14 (7), 4697–4712.